RSC Advances

ROYAL SOCIETY OF CHEMISTRY

www.rsc.org/advances

Journal Name

RSCPublishing

ARTICLE

Effective Near-Infrared-Absorbent: Ammonium Tungsten Bronze Nanocubes

Cite this: DOI: 10.1039/x0xx00000x

Mei Yan, Hongxi Gu, Zhouzhou Liu, Chongshen Guo,* and Shaoqin Liu*

Received 00th January 2012,
Accepted 00th January 2012

DOI: 10.1039/x0xx00000x

www.rsc.org/

Hardly any other compound has realized better optical absorbability of near-infrared-rays (NIR, 780-2500 nm) than tungsten bronze nanoparticles in terms of absorption coefficient, widths of working spectrum, photothermal transformation efficiency and their own physicochemical stability, however, the efforts concerning with the development of tungsten bronzes nanoparticles for serving as NIR absorbent are very limited due to be short of effective approaches to obtain these nanoparticles, especially for the tungsten bronzes with insertion of bigger cations, such as Cs_xWO_3 and $(NH_4)_xWO_3$. In this work, we describe how to fabricate the $(NH_4)_xWO_3$ by a high-temperature but short-time solvothermal process in which involves employing oleic acid/oleylamine as solvent and WCl_6 as W resource, together with inspecting its NIR-absorption related properties. The nanocubes of 100 nm have been characterized by XRD, TG-MS, XPS and TEM to examine the crystal phase and nanostructures. Moreover, the dispersion of nanocubes in the form of thin film was used to investigate the NIR absorption properties. As determined by the optical test, the thin film consisting of nanocubes exhibits extraordinary features as a solar control window, which can transmit the most part of visible light, while absorb nearly all of the NIR rays from 780 nm to 2500 nm. Meanwhile, the $(NH_4)_xWO_3$ thin film can keep high shielding effect for the 1064 nm NIR light up to 35.3 $KW \cdot m^{-2}$ radiation and excellent cyclic stability for 100 cycles without obvious optical change. Finally, it has been found that the $(NH_4)_xWO_3$ nanocubes show remarkable photothermal conversion phenomenon even when dispersed in thin film.

1. Introduction

The near infrared light (NIR) refers to the radiations with wavelength ranging from 780 to 2500 nm, which takes up to 52 % photo-energy of sunlight and is often called heat ray as being perceived by the human body as heat.[1] Actually, the near-infrared region is a burgeoning and unique optical area where the transmittance of radiation is rarely interfered under natural conditions since lacks of the natural NIR absorbent. Development of effective NIR absorbent with a broad working waveband is an advanced hot topic which has significant meaning in improving living conditions of human beings from the viewpoint of photothermal ablation, energy economization, solar collectors, heat-ray shielding smart windows, stealth technology, and optical filters. [2] Over the past decades, it is well known that organic dyes,[3] metal complex with organic ligands,[3] lanthanide boride[4-5] and noble metal nanoparticles[6-13] can realize photoabsorption in the NIR region. However, each of them has their own drawbacks. Optical absorption around 600 - 900 nm originates from the transitions between different energy levels in the molecule for these organic dyes and metal complex with organic ligands, however, the low coefficient of light absorption together with severe photobleaching limit them to be outstanding candidates in this area.[3] Hexaboride nanoparticles absorb only a certain extent wavelengths of NIR rays and are not effective for the whole NIR rays.[4-5] Moreover, reductive atmosphere of the high temperature (ca. 1500 ^oC) is necessary for the syntheses of bulk hexaborides. Afterwards, it exhausts much energy to crush these microsized grains into small nanoparticles because of high hardness. As the variation of surface plasmon resonance, the optical absorption band of noble metal nanoparticles can be readily tuned in the region of 500~880 nm by controlling the shape, size or aspect ratios.[7-13] Despite this advance, development of applicable noble-metal-based NIR absorbent is hurdled by high price, poor scalability and difficulty of obtaining stable powder sample. Additionally, all of the aforementioned compounds only achieve absorption of certain frequencies of NIR light, rather than exhibit strong photoabsorption across the whole NIR region of 780-2500 nm. Therefore, it is extremely urgent to develop effective NIR absorbent with broad working waveband, especially for exploiting oxide-based nanomaterial which shows much better physicochemical stability, more natural abundance and easily to be operated. WO_3-based electrochromic film seems like to be an option regarding the thermal management of windows, but it mainly controls the transmittance of the visible lights by coloring/decoloring cycles instead of controlling on NIR, leading to lower inner brightness on coloring state.

Our previous researches confirmed that, when dispersed as nanosized particles, the hexagonal tungsten bronze type compounds (M_xWO_3, M = Cs, K, Na, Rb, NH_4^+) consisting of mixed chemical valence tungsten ions (W^{6+} and W^{5+}) exhibited excellent NIR absorption properties in a wide range of 780~15000 nm, covering the whole waveband of NIR region and part of Mid-IR area. [14] Among these bronzes, $(NH_4)_xWO_3$ is seldom investigated, which may be related to the great synthetic difficulty originating from high structural distortion of $(NH_4)_xWO_3$ as a result of the insertion of big

NH_4^+ ions into the WO_6 octahedral framework. Designed growth of $(NH_4)_xWO_3$ nanoparticles is of great significance as it also consists of mixed valence tungsten ions being expected to show NIR shielding ability as well. Furthermore, on the merits of its open-tunnel structures and special electronic structure, the mobility of the cations in the channels of the WO_3 framework allows one to dramatically modify the electronic properties by ion exchange or intercalation, giving tungsten bronze of $(NH_4)_xWO_3$ a wide range of related applications as catalytic, battery, gas sensing, and electrochromic materials.[15] Previously, Szila´gyi and his coworkers synthesized the $(NH_4)_xWO_3$ nanoparticles by heating APT in H_2 and confirmed the decomposition temperature for $(NH_4)_xWO_3$ was about 550 ^oC.[16] More recently, colloidal nanocrystals of Cs_xWO_3 were fabricated by Mattox et al via employing oleic acid-oleylamine as solvent at 300 ^oC.[17] Inspired by the above reports, in this work, we synthesized $(NH_4)_xWO_3$ nanocubes under oleic acid-oleylamine medium at a selected temperature of 350 ^oC, which is lower than decomposition temperature of $(NH_4)_xWO_3$, but high enough for rapid fabrication of nanocrystals.

2. Experimental

2.1 Synthesis of $(NH_4)_xWO_3$ nanocubes

Under the standard condition, first, 0.1 g WCl_6 was dissolved into the 8 ml oleic acid to form a yellow solution, to which 2 ml oleylamine was added. Then, the resulting solution was transferred into a batch reactor (Fig. S1) with 20 ml internal volume, and the reactor was sealed and placed in a block heater preheated at 350 ^oC to start the solvothermal reaction. During the heating, the reactors underwent reciprocating shake at a frequency of 50 times/min. After the 1 h reaction, the precipitate was collected by centrifugation, carefully washed with distilled water and ethanol, and dried at 60 ^oC in vacuum overnight to get the final product.(Rinsing precipitates by water is dispensable, but there is negligible effect of water-rinsing on the NIR absorptive performance).

2.2 Characterizations

The phase composition of the sample was determined by X-ray diffraction analysis (XRD, Shimadzu XD-1) using Graphite-monochromized *CuKa* radiation. The size and shape of the nanoparticles were observed by transmission electron microscopy (TEM, JEOLJEM-2010). HRTEM images and SAED images were obtained on ZEISS LEO 922 with an accelerating voltage of 200 kV. The surface composition of the samples and binding energy of W4f were determined by X-ray photoelectron spectroscopy (XPS, Perkin Elmer PHI 5600). XPS date have been calibrated by the C1s line. The thermogravimetric and differential thermal analyses (TG-DTA, riggaku, TG8101D) were performed for the sample from the room temperature to 900 ^oC at a heating rate of 10 ^oC/min in N_2. The atomic force microscopy (AFM, NPX100) measurement was performed for observing the dispersion state of nanoparticles on the film. Surface charge status of the nanorods was examined by zeta-potentials measurement using Nanosizer (Malvern Instruments Ltd., Nano-ZS).

2.3 Optical test

To evaluate NIR absorption characteristics of nanocubes contained thin film, $(NH_4)_xWO_3$ powder was dispersed in collodion - ethanol mixed solution at a mass ratio of ethanol : collodion : powder = 1.0 : 0.93 : 0.15. (The collodion used in this work contains the 10 Wt% of cellulose nitrate and it was purchased from KANTO CHEMICAL CO. INC, Japan.). Then, the coating solution was painted on a quartz glass by an applicator with a concave in depth of 12.5 μm. The optical response of the coating was measured by using a spectrophotometer (JASCO V-670), giving output of transmittance in the UV, visible, and infrared ranges (200 - 2700 nm).
We selected 1064 nm laser as light source and carefully examined the photothermal effect and optical shielding properties of $(NH_4)_xWO_3$ thin film. NIR laser irradiation induced temperature elevation was recorded by a thermographic meter (FLIR System i7).

3. Results and discussion

As shown in TEM image **(Fig.1a)**, the obtained sample mainly consists of many random-distributed rectangular nanoparticles with smooth and dense surface. If we carefully observe the deckle edges of nanocubes, these particles are likely composed by many tiny bundles of nanofibers. In addition, it has observed the aggregation of several nanocubes into big congeries. The particles size distribution reveals a wide size distribution from 40 nm to hundreds nm, however, the most probable value is around 90 nm (Fig.1a Inset), being in agreement with observation in TEM image. The HR-TEM image of certain selected part on single nanocube, shown in Fig.1b, depicts clear lattice fringes, suggesting the nanocubes are well crystallized under 350 ^oC. In addition, the crystalline lattice constant along the nanocube is calculated as 0.378 nm, which agrees well with the interplanar spacing of (0 0 2) of the desired $(NH_4)_{0.33}WO_3$. To provenly validate this, XRD analysis has further been employed to identify the phase composition and crystallographic structure of sample. Figure 1c shows the XRD pattern of as-obtained blue $(NH_4)_xWO_3$ powder, together with standard powder diffraction file of $(NH_4)_{0.33}WO_3$ as reference (JCPDS card No.42-0452). All the reflections shown in Fig.1c could be well indexed as the hexagonal ammonium tungsten bronze with known crystal lattice parameters of a = 0.7392 nm and c = 0.7512 nm, and no characteristic peaks for impurities such as WO_3 or WO_{3-x} were observed. For the hexagonal tungsten bronzes (M_xWO_3, $x \leq 0.33$), the structure mainly comprises a rigid tungsten-oxygen framework built up of layers containing corner-sharing WO_6 octahedron, which are arranged in six-member rings. The layers are stacked along the *c* - axis, leading to formation of one-dimensional open hexagonal channels, which are occupied randomly by cations (Figure 1d).[18] Intercalation of ammonium ions into these channels doubtlessly causes great architectural distortion and tilt, leading to a decrement on the orderliness of crystal unit. This well explains why less successful cases were known to obtain $(NH_4)_xWO_3$ with uniform size or morphology. Next, we carefully examined the chemical composition and chemical state of the $(NH_4)_xWO_3$ nanocrystals by X-ray photoelectron spectroscopy (XPS). A complex energy distribution of W4f photoelectrons was obtained as shown in Fig.1e. After deconvolution, the W4f core-level spectrum could be well fitted into two groups of spin-orbit doublets, corresponding to two different oxidation states of W atoms. The main peaks, giving a W4f 5/2 at 37.7 eV and a W4f 7/2 at 35.6 eV, could be attributed to the W atoms being in a 6+ oxidation state. The second doublet, with a lower binding energy at 34.4 eV and 36.5 eV, could be assigned to the emission of W4f 5/2 and W4f 7/2 core levels from the atoms in an oxidation state of 5+. These results on the core level of tungsten ions are in good agreement with typical nature of tungsten bronze ($M_xW^{6+}_{1-x}W^{5+}_xWO_3$). Although the deconvolution of XPS spectra showed only the presence of W^{5+} and W^{6+} in the sample, we

Journal Name

RSCPublishing

ARTICLE

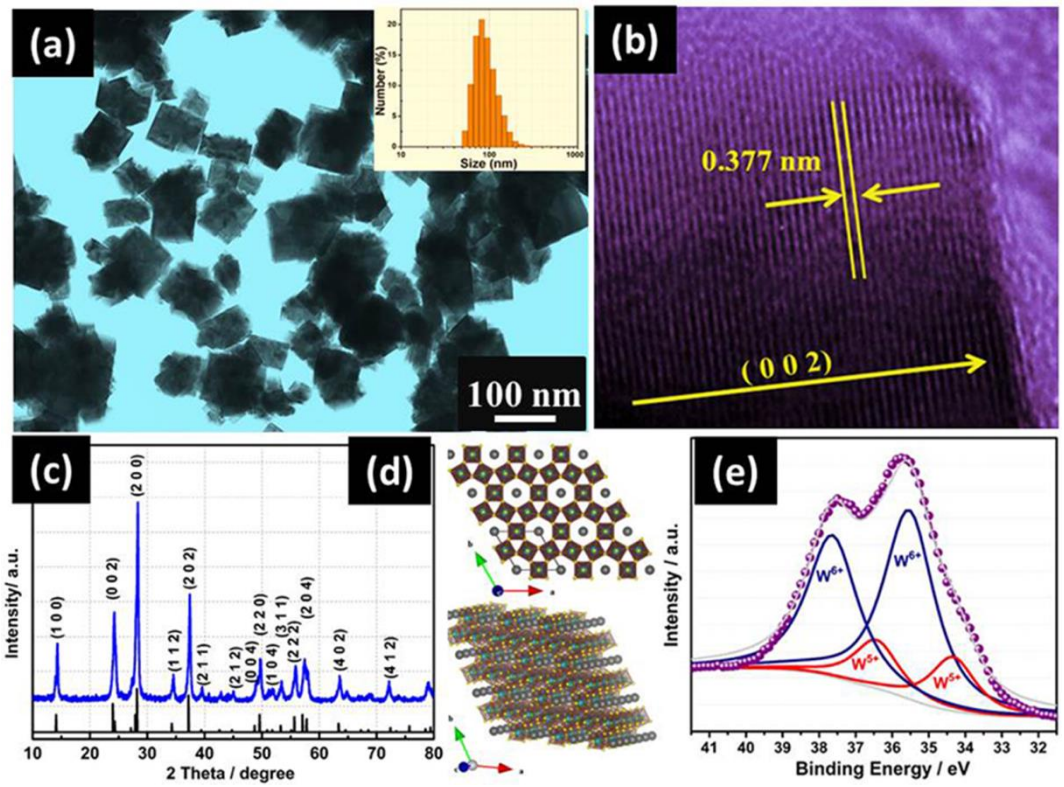

Fig.1 (a) TEM image, (b) HRTEM image, (c) XRD pattern, (d) crystal structure and (e) W4f core-level XPS spectra of obtained $(NH_4)_xWO_3$ nanocubes. Inset of (a) shows corresponding particle size distribution.

can not exclude the presence of trace amount of W^{4+}. Actually, study of Szila´gyi et al has found that there was a small amount of W^{4+} in the reduced tungsten bronze nanoparticles. Due to the presence of W^{5+}, the color of nanocube is dark blue.[16] Other than tungsten, elements of N, O and C (Fig. S2) have been found in the sample as well. The presence of carbon element in the final product may be due to the residual chemically or physically adsorbed organic debris originating from the solvent molecules, while the N element comes from the NH_4^+ in the sample. The chemical composition determined by deconvolution of XPS spectrum is $(NH_4)_{0.25}WO_3$.

The thermal behaviour of $(NH_4)_xWO_3$ nanocube was investigated via thermogravimetry measurement (TG) at a heating rate of 10 ^oC/min, meanwhile, the resulting gas during the heating was flew into the mass spectrum (MS) analyzer to analysis its chemical identity. As shown in **Figure S3**, there are two stages of obvious weight loss, attributing to desorption of water (~ 230 ^oC) and departure of NH_3 from the sample as a result of $(NH_4)_xWO_3$ decomposition (230 - 515 ^oC). This is evidenced by the results of mass spectrometry in which the mass-to-charge m/z (where m is the mass of the ion, and z is the ion charge) ratios of 17, 18 and 28 (Fig.4b), corresponding to the chemical species of NH_3, H_2O, and N_2, respectively, have been found. The observation of $(NH_4)_xWO_3$ decomposition and detection of NH_3 departure by TG-MS method were also observed in other's work.[15] According to the Szila´gyi's report,[19-20] the weight loss at 250-550 ^oC in the TG curve is due to the departure of both NH_3 and NH_4^+ located at the inner site of sample. By calculating the weight loss in this range, we can easily get the total amount of NH_3 and NH_4^+ in the nanocube. On the other side, the content of NH_4^+ could be obtained by XPS spectra. This is because each NH_4^+ ion contributes one electron to the tungsten conduction band, leading to the formation of one W^{5+}. By this way, the chemical formula of nanocube could be expressed as $(NH_3)_{0.05}$ $(NH_4)_{0.25}WO_3$ and the ratio of NH_4^+/NH_3 is 5.

On the basis of aforementioned XRD, XPS and TG results, the obtained nanocube has been well-proven in its phase nature of $(NH_4)_xWO_3$.

The experimental parameters which may influence the crystalline structure of nanoparticle have also been varied to obtain a clear understanding of the crystal growth process under such a reaction system. To clearly validate the role of oleylamine, a series of control experiments with different contents of oleylamine were conducted under the same reaction temperature and period, as well as keeping the total volume of mixed oleylamine-oleic acid solution to be 10 ml. When 1 ml oleylamine was added into the reaction medium, the sample was observed as a mixture of small nanocubes and bundles of nanofibers (Fig.S4). In contrast, the homogeneous oblong

blocks with glossy appearance could be distinguished for the sample synthesized with the assistance of 5 ml oleylamine (Fig.5b). Although the morphologies of samples synthesized with 2 or 5 ml oleylamine addition are very similar to each other (Fig. S4), the yields have drastic differences relative to the content of oleylamine, that is, excessive introduction of oleylamine results in decline of production. This is due to the remarkable pH increment as a result of over-adding oleylamine, which obstructs the formation of powder in that the sufficient acidic condition is necessary for the condensation of dissociative tungsten ions in the solvent into the final tungsten oxides solid. Everything has two sides just like a coin – absence of the oleylamine is unable to produce definite phase of ammonium tungsten bronze, instead, the unknown phase of product was obtained for the sample synthesized in pure oleic acid solution (Fig.S5). Apart from as pH modifier, oleylamine also has been considered as capping agent that plays a vital role in tailoring the nanostructure of nanoparticles. For the $(NH_4)_xWO_3$, we propose that the morphology of the sample depends on the relative growth rates along the *c*-axis (v_c) and lateral side (v_L) to a great extent. In virtue of possessing one-dimensional hexagonal channels along the *c*-axis (Fig.1d), the fastest growth rate is achieved by linking WO_6 octahedra to form these channels along the *c*-axis, and this leads tungsten bronzes to be preferential to grow along the *c*-axis (Fig.S4c upside).[14] Therefore, tungsten bronze nanomaterials have been intensively reported in the one-dimensional form, such as microrods and microfibers, where growth rate along *c*-axis is dominating over that of lateral side.[14] In this work, it has been considered that, selectively absorbing of the oleylamine molecules to crystallographic facets exposed along c-axis slows down the growth rate of v_c to the degree being almost the same to v_L, and results in equivalent growth along both *c*-axis and lateral directions, generating homogenous $(NH_4)_xWO_3$ nanocubes (Fig.S4c). Hence, it is acceptant that, when limited content of oleylamine presents in the reaction system, the oleylamine molecules are not sufficient to cover all the active sites located on every particles and leave part of particles grow into nanofibers freely (Fig.S4a).

In addition to altering the content of solvent, the effects of reaction periods were investigated as well. In fact, the reaction periods have negligible influence on the nanostructure, and the samples after 0.5, 1 and 2 h reaction show almost the same size and shape (Fig. S6), whereas the yield of powder was found to increase from 30% for 0.5 h to above 90% for 1 or 2h.

One of interesting applications for the NIR absorbent is energy-saving windows which should not only shield off the NIR light to prevent indoor temperature increment under strong solar radiation in summer, but also act as heat-insulator to prevent heat-flow escaping from the room in winter. Resultantly, it could reduce the energy consumption for air conditioning and thereby decrease the emission of carbon dioxide. Besides the NIR absorption characters, high visible light transparency is also highly required for these windows to ensure the indoor brightness. In this respect, the optical response of NIR absorbents often is measured in the form of thin film to directly give observation on transparency of visible light and absorptive capacity of NIR irradiations. In this study, the powder sample was mixed with optically transparent binder and coated on the substrate of quartz glass. What need to merit special attention, the blue coating just consists of 7.7 wt% $(NH_4)_xWO_3$ nanocubes, while the rest part is polymer binder. As shown in Fig.2a, the coated film is tinted blue, but is highly transparent. For investigating the dispersion sates of $(NH_4)_xWO_3$ nanoparticles on the surface of film, the AFM technique was performed to provide more details on coated film. As shown in Fig. 2b, 2D AFM image clearly reveals that the surface layer of film is covered homogenously by many flocculent globoids with diameters in the range of 0.5 - 1 μm, which is much bigger than the size of nanocube of 100 nm shown in Fig.1a, indicating that the globoid is the aggregation of nanoparticles and binder part. The surface layer of film is uniform and smooth as shown in Fig.2c, with a mean interface roughness (Ra) of 44.2 nm. In addition, the thickness of the tinted film was around 1 μm.

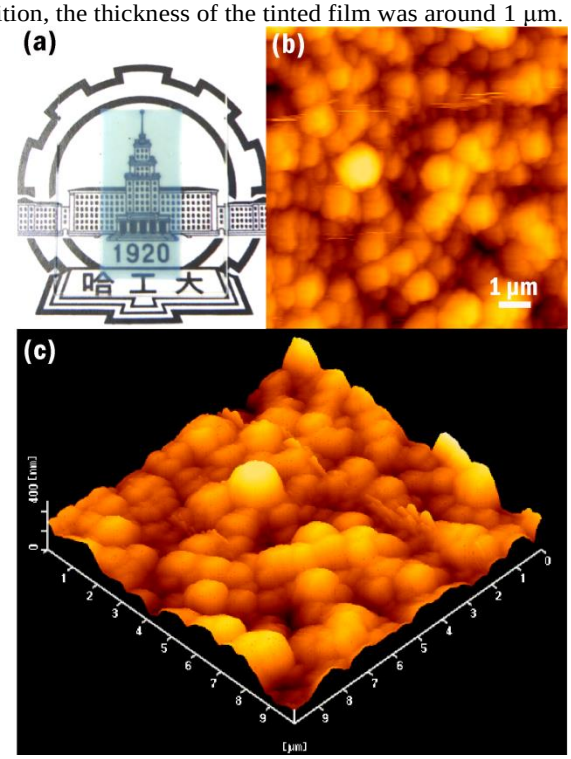

Figure 2 (a) Photograph of thin film with dispersion of $(NH_4)_xWO_3$ nanocubes; (b) 2D and (c) 3D AFM images of the film coated on the quartz.

Figure 3 exhibits the transmittance spectra of thin film being composed of $(NH_4)_xWO_3$ nanocube. For the NIR absorptive properties, it is closely related to the free electrons originating from W^{5+} or W^{4+}.[14] For comparison, we also tested the optical performance of the h-WO_3 showing similar hexagonal channels to $(NH_4)_xWO_3$ but differing in fully oxidized state and low occupancy, and $(NH_4)_xWO_{3+x/2}$ only differing in fully oxidized state ($(NH_4)_xWO_{3+x/2}$ was synthesized according to ref. 21). Apparently, the relevant homologues of hexagonal h-WO_3 and$(NH_4)_xWO_{3+x/2}$ are transparent for the NIR irradiation and visible light (Fig.3a and b), indicating there is no obvious absorptive abilities for these two species. The commercial $Cs_{0.33}WO_3$ possessing similar chemical composition and valence to $(NH_4)_xWO_3$ nanocubes of this work was treated under same conditions. It can be seen that the thin film consisting of commercial microsized $Cs_{0.33}WO_3$ can shield off about 50% NIR light (Fig.3d). In sharp contrast, as shown in Fig.3c, the $(NH_4)_xWO_3$ nanocubes coated film selectively transmits the majority of visible lights in the range of 400 - 800 nm, as well as cuts off the near infrared and UV lights effectively. The transmittance of NIR light is lower than 20%. Meanwhile, the reflectance characters shown in Fig.3d clearly reveal that the light scattering on the thin film is very limited in the whole region of 200-2700 nm. For the optical response of

thin film, 100% - T - R is photo-absorptivity, where T is transmittance of light and R is reflectance happened on the surface of coating. In this work, the low reflectance and transmittance in the NIR region for $(NH_4)_xWO_3$ nanocube of this work manifest its outstanding NIR absorptive ability. The luminous efficiency function describes the average spectral sensitivity of human visual perception of brightness according to the light of different wavelengths (black area). It can be seen that the maximum transmittance of $(NH_4)_xWO_3$ film in the visible region overlaps with area of luminous efficiency function, suggesting the film can selectively transmit the visible light which is more bright among the visible spectrum.

On the basis of above results, one can conclude that, for realization of NIR absorption, low valence state of W^{5+} and smaller size are highly required. This can well explain why the $(NH_4)_xWO_{3+x/2}$ consisting of W^{6+} only did not show any NIR absorptive character and $Cs_{0.33}WO_3$ with W^{5+} but microsize showed weaker NIR absorption.

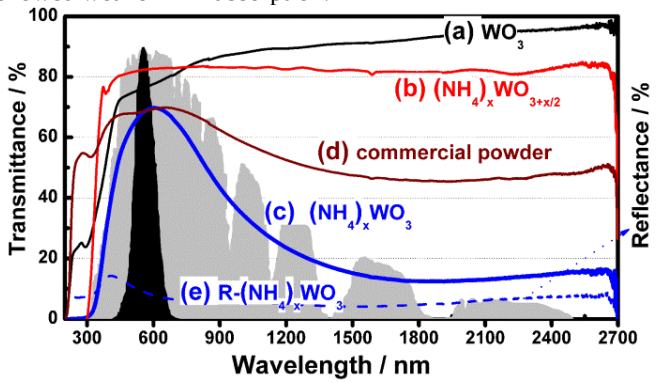

Figure 3 Transmittance spectra of thin films containing (a)h-WO_3, (b) $(NH_4)_xWO_{3+x/2}$, (c) $(NH_4)_xWO_3$ nanocube of this work; (d) commercial powder of $Cs_{0.33}WO_3$. (e) reflectance profiles of film containing $(NH_4)_xWO_3$ nanocube. The black and gray areas indicate the normalized value of the luminous efficiency function and energy wavelength distribution of solar spectrum on the sea level.

In addition, we also have measured the optical absorbance of powder sample to give direct judgment on intrinsic optical absorptive ability. It is further revealed that the $(NH_4)_xWO_3$ blue powder can strongly absorb the NIR light from 780 nm to 2500 nm (Fig.S8).

For further investigating the feasibility of employing $(NH_4)_xWO_3$ film as NIR resisting coating, we tested its shielding properties for 100 cycles at selected power density of 442.32 W/m^2 and 4423.2 W/m^2, which are close to density of NIR light contained in sunlight and tenfold power of NIR light contained in sunlight, respectively. The percent transmittancy in presence or absence of $(NH_4)_xWO_3$ film as well as related time response under two powder densities are shown in Fig.4. The optical transmittance decreases from 100 % to 20% under 442.32 W/m^2 irradiation and to 25% under 4423.2 W/m^2 irradiation (corresponding to shielding off 75-80% NIR light) as soon as (within 2 second) setting film on the light path and then recovers soon as removing the film. Notably, high cyclic stability was observed under two powder densities as the transmittance switching responses for the first 10th and last 10th are nearly the same and no obvious optical change appeared. These positive results stimulate us to investigate the cyclic stability at even higher NIR laser irradiations. By successively stepping up the input power density of NIR light, one can find that $(NH_4)_xWO_3$ film can maintain stable shielding percentage of NIR light up to 35.3 KW•m^{-2} disregarding the powder density,(Fig.S9) and the destruction of polymer binder part in the film happened when density overstepped this limitation. In brief, $(NH_4)_xWO_3$ film exhibits desirable photostability on the merit of its oxide nature.

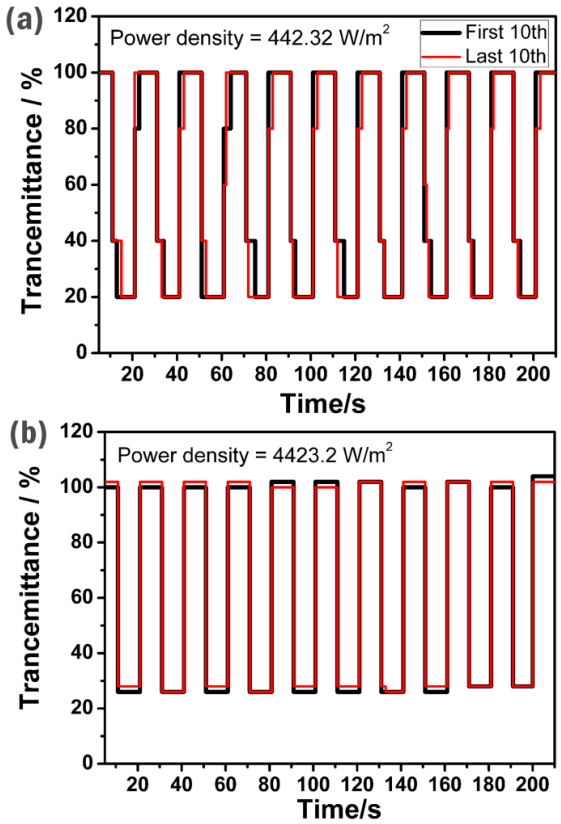

Figure 4 Transmittance switching response of $(NH_4)_xWO_3$ film irradiated by (a) 442.32 W/m^2 and (b) 4423.2 W/m^2 of 1064 nm light. The $(NH_4)_xWO_3$ film was set on the light path for 10 s and then taken out for repeated 100 cycles. Black and red curves represent the transmittance switching response for first 10th and last 10th cycles, respectively.

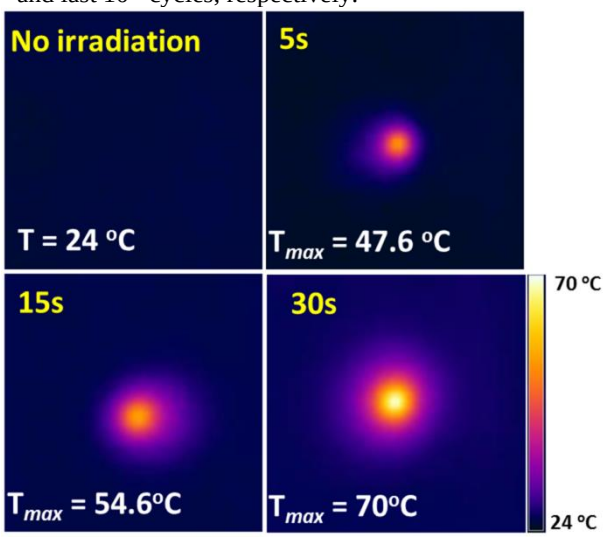

Figure 5 The temperature variation of $(NH_4)_xWO_3$ film as radiation duration.(The film was irradiated by 1064 nm laser at power density of 17.7 KW•m^{-2}).

During the test, we also found that there was obvious photo-thermal conversion effect on the irradiation area of film. As is shown in Fig.5, the temperature of central irradiation area monitored by thermographic survey increases from ambient 24 ^{o}C to 47.6, 54.6 and 70 ^{o}C, after 5, 15, 30 second exposure to the 1064 nm laser, respectively. Meanwhile, as a result of thermal diffusion from the centre, the area of hot zone becomes larger as increment in radiation duration.

Conclusions

In summary, we have presented a new one-step strategy to obtain ammonium tungsten bronze that has never been fabricated in the form of nanocubes. Characterization results suggested that the obtained sample was pure phase of tungsten bronze with mixed chemical valence of W^{5+} and W^{6+}. The optical tests revealed that the $(NH_4)_xWO_3$ nanocube can strongly absorb the NIR light from 780 to 2500 nm either as powder or dispersed as thin film. Remarkably, thin film of $(NH_4)_xWO_3$ nanocube showed excellent cyclic stability even after 100 cycles and efficient NIR shielding performance against nearly 90-fold density of NIR light contained in sunlight. Due to the high efficiency of absorption of NIR light, $(NH_4)_xWO_3$ nanocube also exhibited instantaneous opt-thermal conversion upon NIR irradiation. Therefore, the resulting $(NH_4)_xWO_3$ nanocube is anticipated to be upcoming potent candidate as NIR absorbent with wide response range, high absorptivity and cyclic stability.

Acknowledgements

The financial supports from National Basic Research Program of China (2013CB932704), National Natural Science Foundation of China (Grant No. 21303033, 81373359, 91023007 and 20773033), New Century Excellent Talents in University, Outstanding Young Funding of Heilongjiang Province were gratefully acknowledged. This work is also supported by "the Fundamental research Funds for the Central Universities" (Grant No. HIT. NSRIF.2015061&2015062), Heilngjiang Postdoctoral Financial Assistance (Grant No. LBH-Z13079) and China Postdoctoral Science Foundation Funded Project (Project No.: 2014M551232&2014M551224).

Notes and references

Key Laboratory of Microsystems and Micronanostructures Manufacturing (Ministry of Education), Harbin Institute of Technology, Harbin 150080, China.
E-mail: shaoqinliu@hit.edu.cn; chongshenguo@hit.edu.cn

Electronic Supplementary Information (ESI) available: [XRD pattern, Zeta potential, TEM image of samples, Optical absorbance of powder]. See DOI: 10.1039/b000000x/

1 C. S. Guo, S. Yin, L. J. Huang, L. Yang and T. Sato, *Chem. Commun*., 2011, **47**, 8853.
2 C. S. Guo, S. Yin, Y. F. Huang, Q. Dong and T. Sato, *Langmuir*, 2011, **27**, 12172.
3 J. Faban, *Chem. Rev*., 1992, **92**, 1197.
4 H.Takeda and K.Adachi, *J. Am. Ceram. Soc.*, 2007, **90**, 4059.
5 K. Adachi and M.Miratsu, *J. Mater. Res.*, 2010, **25**, 3.
6 K. W. Hu, T. M. Liu, K. Y. Chung, K. S. Huang, C. T. Hsieh, C. K. Sun and C. S. Yeh, *J. Am. Chem. Soc*., 2009, **131**, 14186.
7 B. Jang, J. Y. Park, C. H. Tung, I. H. Kim and Y. Choi, *ACS Nano*, 2011, **5**, 1086.
8 H. C. Huang, K. Rege and J. J. Heys, *ACS Nano*, 2010, **4**, 2892.
9 Z. J. Zhang, L. M. Wang, J. Wang, X. M. Jiang, X. H. Li, Z. J. Hu, Y. H. Ji, X. C. Wu and C. Y. Chen, *Adv. Mater*., 2012, **24**, 1418.
10 L. R. Hirsch, R. J. Stafford, J. A. Bankson, S. R. Sershen, B. Rivera, R. E. Price, J. D. Hazle, N. J. Halas and J. L. West, *P. Natl. Acad. Sci. USA.*, 2003, **100**, 13549.
11 L. Gao, J. B. Fei, J. Zhao, H. Li, Y. Cui and J. B. Li, *ACS Nano*, 2012, **6**, 8030.
12 Y. N. Xia, W. Y. Li, C. M. Cobley, J. Y. Chen, X. H. Xia, Q. Zhang, M. X. Yang, E. C. Cho and P. K. Brown, *Acc. Chem. Res.*, 2011, **44**, 914.
13 X. Huang, S. Tang, X. Mu, Y. Dai, G. Chen, Z. Zhou, F. Ruan, Z. Yang and N. Zheng, *Nature Nanotechnology*, 2011, **6**, 28.
14 C. S. Guo, S. Yin, P. L. Zhang, M. Yan, K. Adachi, T. Chonan and T. Sato, *J. Mater. Chem*., 2010, **20**, 8227.; C. S. Guo, S. Yin, M. Yan and T. Sato, *J. Mater. Chem.*, 2011, **21**, 5099.; C. S. Guo, S. Yin and T. Sato, *Nanosci. Nanotechnol. Lett.*, 2011, **3**, 413.; C. S. Guo, S. Yin, L. J. Huang and T. Sato, *ACS Appl. Mater. Interfaces*, 2011, **3**, 2794. ; C. S. Guo, S. Yin, Q. Dong and T. Sato, *CrystEngComm*, 2012, **14**, 7727.
15 C. S. Guo, S. Yin, and T. Sato, *Rev. Adv. Sci. Eng*., 2012, **1**, 235.
16 I. M. Szila ́gyi, J. Madara ́sz, G. Pokol, P. Kira ́ly, G. Ta ́rka ́nyi, S. Saukko, J. Mizsei, A. L. To ́th, A. Szabo ́, and K. V. Josepovits, *Chem. Mater*. 2008, **20**, 4116.
17 T. M. Mattox, A. Bergerud, A. Agrawal, and D. J. Milliron, *Chem. Mater*. 2014, **26**, 1779.
18 D. W. Lynch, R. Rosei, J. H. Weaver and C. G. Olson, *J. Solid State Chem.*, 1973, **8**, 242.
19 I. M. Szila ́gyi, J. Madara ́sz, G. Pokol, F. Hange, G. Szalontai, K. V. Josepovits and A. L. To ́th, *J. Therm. Anal. Cal.*, 2009, **97**, 11.
20 I. M. Szila ́gyi, I. Sajo ́, P. Kira ́ly, G. Ta ́rka ́nyi, A. L. To ́th, A. Szabo, K. V. Josepovits, J. Madara ́sz and G. Pokol, *J. Therm. Anal. Cal.*, 2009, **98**, 707.
21 C. S. Guo, S. Yin, Y. Huang, Q. Dong and T. Sato, *Langmuir*, 2011, **27**, 12172.

The thin film consisting of $(NH_4)_xWO_3$ nanocubes can transmit the most part of visible light, while absorb nearly all of the NIR rays from 780 nm to 2500 nm, as well as showing remarkable photothermal conversion phenomenon even when dispersed in thin film.